Loss of nitrogen via anaerobic ammonium oxidation (anammox) in the California current system during the late Quaternary

Zoë Rebecca van Kemenade [1], Zeynep Erdem [1], Ellen Christine Hopmans [1], Jaap Smede Sinninge Damsté [1,2], Darci Rush [1]

[1] NIOZ Royal Netherlands Institute for Sea Research, PO Box 59, 1790 AB, Den Burg, The Netherlands
[2] Department of Earth Sciences, Utrecht University, Princetonlaan 8a, 3584 CB, Utrecht, the Netherlands

Correspondence to: Zoë R. van Kemenade (zoe.van.kemenade@nioz.nl)

Abstract. The California current system (CCS) hosts one of the largest oxygen minimum zones (OMZs) in the world: the Eastern North Pacific (ENP) OMZ, which is dissociated into a subtropical and tropical region (i.e., the ESTNP and ETNP). In the modern ENP OMZ, bioavailable nitrogen (N) is lost via denitrification and anaerobic ammonium oxidation (anammox). Even so, paleo-reconstructions of N-loss have focused solely on denitrification. Fluctuations in bulk sedimentary $\delta^{15}N$ over glacial-interglacial cycles have been interpreted to reflect variations in denitrification rates in response to ETNP OMZ intensity changes. This $\delta^{15}N$ signal is thought to be transported northwards to the ESTNP OMZ. Here, we present the first CCS sedimentary record of ladderane lipids, biomarkers for anammox, located within the ESTNP OMZ (32°N; 118°W). Over the last two glacial terminations (~160 cal ka BP), ladderane concentrations were analysed in combination with the index of ladderanes with five cyclobutane moieties (NL_5), short-chain (SC) ladderane degradation products, and productivity proxies. This shows that: 1) ladderanes derived from anammox bacteria living within the ESTNP OMZ water column; 2) ladderanes were continuously present, with relatively high concentrations during both glacial- and interglacial-periods, showcasing the ESTNP OMZ must have retained an anoxic core in which N-loss occurred; and 3) anammox abundance appears to have been driven both by OM-remineralization and advection changes, which regulated nutrient and oxygen levels. Our study shows that anammox was an important feature in the CCS and provides a more holistic picture of N-loss dynamics and the development of the ESTNP OMZ over glacial-interglacial cycles. Lastly, ladderanes and their SC-products were also detected in 160–500 cal ka BP sediments (15.7–37.5 mbsf; analysed at a low temporal resolution), highlighting their potential as anammox biomarkers in relatively deeper buried sediments for future studies.

1 Introduction

The California current system (CCS) is one of four major Eastern Boundary upwelling systems (EBUS). In EBUS, wind-driven offshore advection of surface waters causes deeper, cold, nutrient-rich waters to be upwelled into the photic zone, fuelling primary productivity (e.g., Bakun and Nelson, 1991). Consequently, the CCS is one of the world's most productive oceanic regions, with year-round upwelling, resulting in high primary production rates (Huyer, 1983; Dorman and Winanat, 1995). In the CCS, the respiration of sinking organic matter (OM), in combination with limited ventilation of the North Pacific intermediate waters (Reid and Mantyla, 1978; Sonnerup et al., 1999; Fine et al., 2001), results in the formation of the

Eastern North Pacific oxygen minimum zone (ENP OMZ). The ENP is divided into the Eastern tropical North Pacific (ETNP) and Eastern subtropical North Pacific (ESTNP) OMZs.

The suboxic/anoxic conditions of OMZs cause the marine nitrogen (N) cycle to shift towards two processes that result in the loss of bioavailable N through the production of dinitrogen gas (N_2): 1) anaerobic ammonium oxidation (anammox) and 2) denitrification. Anammox is the oxidation of ammonium (NH_4^+) to N_2 using NO_2^- as the terminal electron acceptor (van de Graaf et al., 1997, 1995), and is performed in the marine water column by anammox bacteria of the genus '*Ca.* Scalindua' (Kuypers et al., 2003). Anammox bacteria are chemolithoautotrophs and use carbon dioxide (CO_2) as their carbon source. Denitrification is the stepwise reduction of nitrate (NO_3^-), to nitrite (NO_2^-), to N_2 (Kuenen and Robertson, 1987) and is performed by a wide range of organisms, most of which are heterotrophs. During denitrification, nitrous oxide (N_2O) can be released as an intermediate product (Kuenen and Robertson, 1987), which has a global warming potential 265 times that of CO_2 (Vallero, 2019).

While permanent OMZs contribute to only 8 % of the total oceanic area (Paulmier and Ruiz-Pino, 2009), they are responsible for 20–50 % of total global N loss (Gruber, 2004; Codispoti et al., 2001). Decreased N availability in OMZs may limit primary producers, and hence, the uptake of CO_2 into the organic matter (OM) pool. This may reduce the efficiency of the ocean's biological pump, which exports organic C from the euphotic zone to the sea floor. Thus, OMZs not only have a disproportionately large impact on the marine nitrogen cycle, but changes in N-loss dynamics may also feed back into the carbon cycle.

The ENP OMZ is expanding both vertically (shoaling towards the ocean's surface; Bograd et al., 2008) and horizontally (Zhou et al., 2022) with present-day climate change. This follows observed trends of overall deoxygenation of the North Pacific since the 1960's (Whitney et al., 2007; Stramma et al., 2010; Pierce et al., 2012; Smith et al., 2022), linked to anthropogenically-induced ocean warming as a response to increased greenhouse gas emissions (Laffoley and Baxter, 2019). As a result of the decreasing dissolved oxygen (DO) concentrations, denitrification has been shown to increase in the North Pacific over the last decades (Peters et al., 2018; White et al., 2019). Vertical expansion and intensification of the ENP OMZ have also occurred in the absence of anthropogenic influences in the past, as recorded by redox-sensitive trace metals in the sedimentary archive (Wang et al., 2020). This is thought to be caused by changes in DO concentrations during glacial-interglacial transitions (terminations). Model simulations indicate that during glacials, cooling of the polar regions led to a more restrained and intensified Hadley cell (Nicholson and Flohn, 1981). This is thought to have caused southward transport of high-oxygen, nutrient-rich North Pacific Intermediate Water (NPIW; Herguera et al., 2010) and limited northward advection of the warm, oxygen-poor California undercurrent (CU), resulting in a more oxygenated OMZ. During interglacials, the oxygen deficiency in the OMZ is thought to have increased due to enhanced advection of the warm, oxygen-depleted waters of the CU originating from the tropics ((Lembke-Jene et al., 2018; Hendy and Kennett, 2003), water

column stratification (Wang et al., 2020), and enhanced upwelling of nutrient-rich waters (Choumiline et al., 2019). These previous glacial-interglacial transitions may be considered as analogues for the effect of future climate change on the N-cycle.

In the CCS, enriched isotope ratio values of bulk sedimentary nitrogen ($\delta^{15}N$) during interglacial periods have been interpreted to reflect increased denitrification in response to OMZ intensification (e.g., Kienast et al., 2002; Kemp et al., 2003; Liu et al., 2005). Sedimentary $\delta^{15}N$ values are governed by the isotopic fractionation (ε) induced by biological transformations and can be used to infer past N-cycling. For water column denitrification, the production of N_2 induces an isotope fractionation effect of +20 to +30 ‰ on the residual nitrogen (Ryabenko, 2013; Sigman and Fripiat, 2019). Enrichment cultures of anammox bacteria have, however, shown that they induce a similar isotope fractionation effect (Brunner et al., 2013), with that of *Ca.* Scalindua spp. being +16 to +30 ‰ (Kobayashi et al., 2019). Although anammox occurs in the modern North Pacific oxygen deficient waters (Rush et al., 2012a; Peng et al., 2015; Sollai et al., 2015; Hamasaki et al., 2018), and anammox is reported to be the dominant N-loss process in the Eastern Tropical South Pacific (ESTP; Galán et al., 2009; Thamdrup et al., 2006; Hamersley et al., 2007), to the best of our knowledge, there are no reconstructions on the occurrence of anammox in the sediment archive of the CCS. Moreover, a long-standing conundrum is the discrepancy between the timing of enriched $\delta^{15}N$ values, and enhanced marine productivity, especially north of the ETNP (Kienast et al., 2002), suggesting a decoupling between remineralization rates and N-loss (Ganeshram et al., 2000).

While sedimentary $\delta^{15}N$ values are shaped by the sum of N-cycling processes, lipid biomarkers provide more detailed information (see Rush and Sinninghe Damsté, 2017 for a review). Anammox bacteria biosynthesise C_{18} and C_{20} ladderane fatty acids (FAs) (Fig. 1). These unique lipids contain three or five linearly concatenated cyclobutane rings ([3]-ladderane and [5]-ladderane, respectively; Sinninghe Damsté et al., 2002). Ladderanes have been successfully applied to trace abundances of *Ca.* Scalindua spp. in the modern ENP water column (Rush et al., 2012a; Sollai et al., 2015) and as anammox biomarkers in sedimentary records up to 140 ka (Jaeschke et al., 2009; Rush et al., 2019; van Kemenade et al., 2023). Moreover, during exposure to oxic conditions ladderane FAs undergo microbially-mediated oxic degradation of the alkyl side chain by β-oxidation, in which C_{18}- and C_{20}-ladderane FAs are sequentially transformed into the short-chain (SC) C_{16}- and C_{14}-ladderane partial degradation products (Rush et al., 2011, 2012b). Thus, SC-ladderane FAs in the sediment archive may be used to trace back anammox cell material that has been exposed to oxic conditions, such as sedimentation through the oxic water underlying an OMZ. Furthermore, the index of ladderane FAs with five cyclobutane rings (NL_5) has been shown to correlate with the *in situ* water temperature at which ladderane FAs are synthesised (Rattray et al., 2010), which has been used to determine the provenance of ladderane lipids (Jaeschke et al., 2009; Rush et al., 2012a; Van Kemenade et al., 2022).

92   Here, we describe the occurrence of ladderane FAs in a ~160 cal ka BP sediment record from the CCS, covering the

93   two most recent glacial terminations (T1 and T2). We combined (SC-)ladderanes and the NL_5 index with sedimentary bulk

94    $\delta^{15}N$, stable carbon isotope ratio ($\delta^{13}C$), total organic C (TOC) and total N (TN) to investigate the feedback of changing

95   OMZ intensity on the occurrence of anammox within the CCS. Moreover, ladderane FAs were also investigated, albeit in

96   low-resolution, in >160 cal ka BP sediments (up to 500 cal ka BP) to explore their preservation potential.
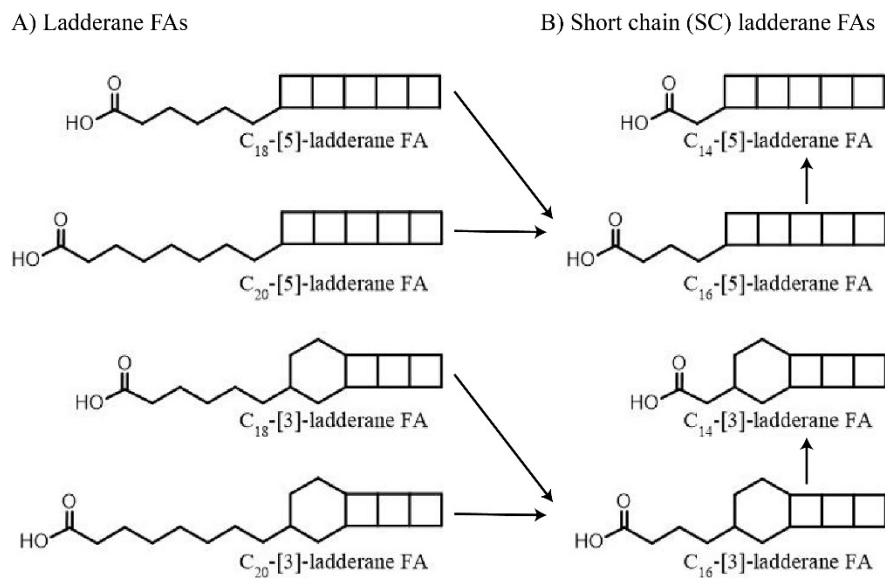
98   **Figure 1**: Structures of anammox lipid biomarkers used in this study: A) ladderane fatty acids (FAs) with 5 or 3 cyclobutane moieties

99   containing 18 or 20 carbon atoms. B) short chain ladderane fatty acids (FAs) with 5 or 3 cyclobutane moieties containing 16 or 14 carbon

100   atoms. Proposed diagenetic pathways are indicated using black arrows (adapted from Rush et al., 2011).

101   **2 Hydrographic setting**

102   The northern boundary of the CCS is at the transition zone between the North Pacific Current (NPC) and Alaska gyres

103   (~50°N) and is bordered in the south by the subtropical waters of Baja California, Mexico (~15–25°N). The CCS (Fig. 2A) is

104   shaped by: (i) the equatorward California current (CC), extending roughly 1000 km off the North American coast (Checkley

105   and Barth, 2009), (ii) the poleward, near-shore flowing CU, and (iii) the seasonal poleward flowing Davidson current (DC).

106   The CC is a year-round, cold, low-salinity, nutrient-rich surface current (<300 m below sea surface; mbss), originating from

107   the North Pacific Current. While the CC is strongest in spring and summer, the DC originating around Point Conception

108   (35°N) dominates the surface-flow throughout winter. The deeper waters of the CC are shaped by the NPIW (300–800

109   mbss), which circulates clockwise in the North Pacific gyre (Sverdrup et al., 1942) and is carried southwards by the CC.

110   Around Baja California, it convolutes with unventilated intermediate waters of tropical origin, which have been transported

111   to the eastern Pacific by the Equatorial undercurrent (EUC; Reid, 1997; Reid and Mantyla, 1978). Here, part of the CC turns

112   north to become the CU. The CU (~100–300 mbss) carries the warm, high-salinity, low oxygen waters from Baja California

towards Vancouver Island (Thomson and Krassovski, 2010). Within the CCS, the geostrophic flow of the CC in combination with Ekman transport and eddy activity cause an offshore transport of (sub-)surface waters and strong coastal jets, which are replaced by the upwelling of the nutrient-rich undercurrent waters (Huyer, 1983; Chavez and Messié, 2009). Upwelling occurs year-round, and results in high primary production (Bograd et al., 2009). In the CCS, the high organic matter flux, together with the poor ventilation of the intermediate-water mass (Reid and Mantyla, 1978; Fu et al., 2018), results in the formation of the ENP OMZ, disassociated in the ETNP (0–25°N; 75–180°W) and ESTNP (25–52°N; 75–180°W) (Fig. 2B). Dissolved oxygen (DO) concentrations in the cores (<20 μmol kg^{-1}) of both the ETNP (~320–740 meters below sea surface, 'mbss') and ESTNP (~850–1080) OMZ decrease below <1 μmol kg^{-1} (Palmier and Ruiz-Pino, 2009) (Fig. 2C).

3 Methods

3.1 Sampling location and strategy

The sediment record was recovered in 1996 during Ocean Drilling Program (ODP) Leg 167 (Lyle et al., 1997) . Site 1012 is located 105 km offshore California in the East Cortez Basin (32°16.970′N, 118°23.039′W), near the southern front of the CC and northern front of the ETNP OMZ (Fig. 2B). The core was recovered from a water depth of 1784 m below sea surface (mbss). For this study, 69 sediment depths (volumes of 20 cm^3) were selected for ladderane FAs analysis. Sedimentation rates ranged from 4 to 15 cm kyr^{-1} (S1, Table 1). Considering the oldest detected ladderane FAs were in 140 ka BP sediments (~10 m below sea floor 'mbsf') of the Arabian Sea (Jaeschke et al., 2009), we subsampled at a higher resolution (every 10 to 50 cm) to the first ~160 kyr (15.7 mbsf) of the record (with a maximum resolution of 10 cm around T1 and T2) and at a lower resolution (80 to 200 cm) to ~500 cal ka BP (37.5 mbsf). In addition, 74 sediments (10-50 cm resolution) were analysed for bulk sedimentary organic carbon (TOC) and N (TN) content, the C/N ratio (atomic) and bulk isotopic ratio values (δ^{15}N and δ^{13}C). A detailed overview of all samples is given in Supplement 1, Tables 1 and 2. Samples were freeze-dried and stored at -20 °C prior to analysis.

3.2 Analysis of sedimentary bulk TOC, TN, C/N, δ^{13}C and δ^{15}N

Sediments were freeze-dried and ground to powder. For TOC and δ^{13}C analysis, aliquots of bulk sediment were decalcified to remove all carbonates. Samples were first acidified with 2M hydrochloric acid (HCl) and rinsed with distilled water to remove the salts. After the decalcification step, ca. 0.5 mg of dried material was used for the analysis. For TN and stable nitrogen isotope ratio (δ^{15}N) between 15 and 20 mg of non-decalcified sediment were used. All samples were packed in tin cups and introduced to the Thermo Scientific Flash 2000 elemental analyzer coupled to a Thermo Scientific Delta V Advantage isotope ratio mass spectrometer (EA/IRMS). Results are expressed in standard notation relative to Vienna Pee Dee Belemnite (VPDB) for δ^{13}C and relative to air for δ^{15}N. The precision as determined using laboratory standards

142 calibrated to certified international reference standards was in all cases < 0.2 ‰. The sedimentary C/N ratios (based on total

143 organic C and total N) were calculated using their atomic mass.
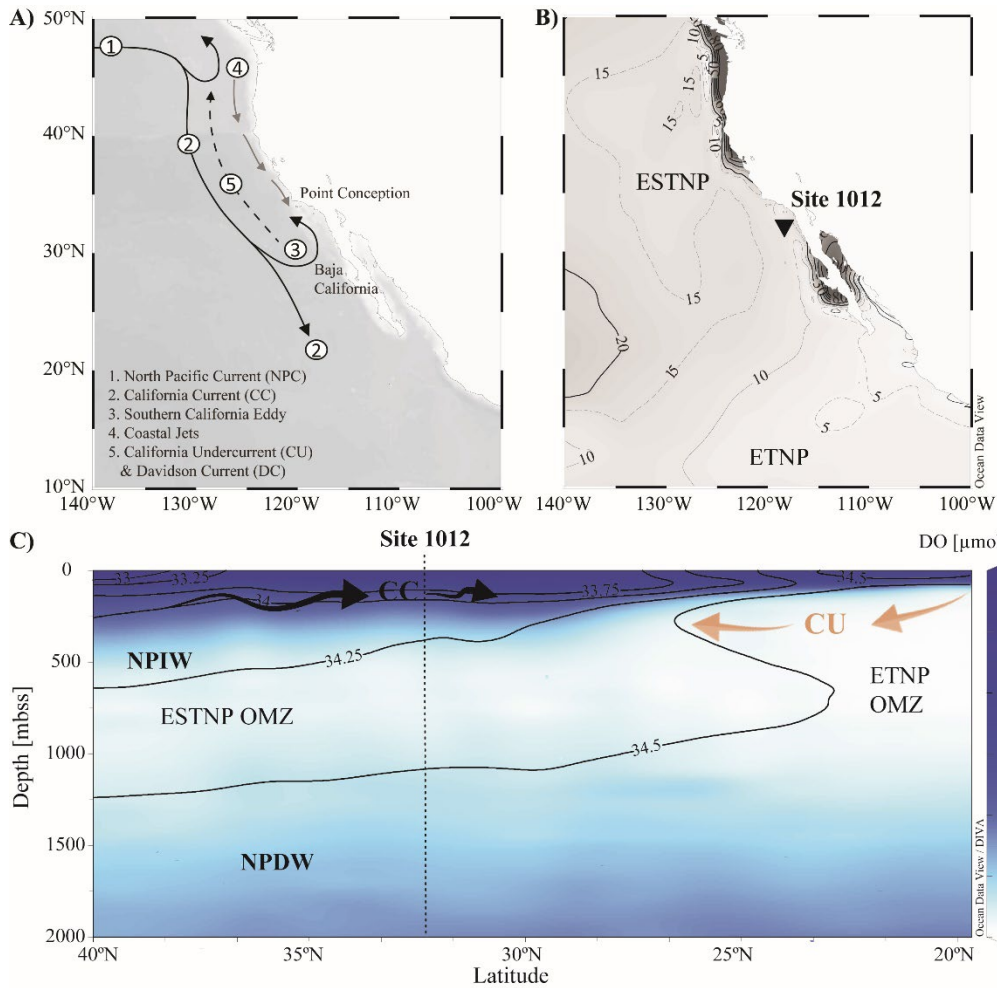
145 **Figure 2:** A) map of the California Current System (CCS). Key currents are indicated with arrows. B) location of ODP site 1012

146 (32°16.970′N; 118°23.039′W) recovered at 1784 mbss, with minimum dissolved oxygen (DO) concentrations [μmol kg⁻¹] detected in the

147 water column in 2018 (WOA, 2018). C) A latitudinal section plot of the CCS water column showing modern annually averaged DO (μmol

148 kg⁻¹) concentrations and salinity (psu) concentrations with the color bar and contour lines, respectively (WOA, 2018). Major current and

149 water masses are also indicated, i.e., the Eastern Tropical and Eastern Subtropical North Pacific (ETNP and ESTNP, respectively) OMZs,

150 the California Current (CC; black arrows), the California Undercurrent (CU; orange arrows), North Pacific intermediate waters (NPIW)

151 and North Pacific deep water (NPDW). Maps were created in Ocean Data View and DIVA gridding was applied for interpolation of DO

152 concentrations (Schlitzer and Reiner, Ocean Data View, 2021).

153 **3.3 Age model**

154 Liu et al. (2005) previously constructed an age model for ODP site 1012, based on sediments recovered from Hole B. As the

155 material used in this study is predominantly from Hole A and C, a revised age model was constructed (S1, Table 1). The

156 revised age model for sediments up to 160 cal ka BP (15.7 m composite depth, 'mcd') was created by correlation of the bulk

157 sedimentary $\delta^{15}N$ record of Liu et al., (2005) with our dataset. Tie points (age *vs* composite depth) were selected by fine-

158 tuning using QAnalyseries (version 2022). For sediments >160 cal ka BP, which were solely sampled for ladderane FAs at

159 low resolution (i.e. not sedimentary $\delta^{15}N$), the age model of Liu et al. (2005) is used.

160 **3.4 Ladderane extraction**

161 Homogenized, freeze-dried sediments were extracted using a low temperature - low pressure accelerated solvent extraction

162 (ASE) method, previously described for ladderane extraction in Rush et al. (2012b). Thereafter, aliquots of the total lipid

163 extract were saponified in 2 N potassium hydroxide (in a 96 % MeOH solution) by refluxing for 1 h. After, 2 mL of

164 bidistilled water was added. The saponified extracts were acidified by adjusting the pH to 3 with 2 N hydrochloric acid (in a

165 50 % MeOH solution). Phase separation was induced by adding 2 mL of DCM. The biphasic mixtures were sonicated for 5

166 min and centrifuged for 2 min (3000 rpm). The DCM layers, containing the FAs, were collected. The mixtures were

167 partitioned twice more with DCM, after which the same procedure was applied before collection of the DCM layers. The FA

168 fractions were dried over a sodium sulphate (Na_2SO_4) column. Then, the fractions were methylated with diazomethane to

169 convert FAs into their corresponding fatty acid methyl esters (FAMEs) and allowed to airdry overnight to avoid losing the

170 more volatile SC-ladderane FA had they been dried under a stream of N_2. The methyl esters of the polyunsaturated fatty

171 acids (PUFAs) were removed by eluting the FAME fractions with DCM over a silica impregnated silver nitrate ($AgNO_3$)

172 column. FAME fractions were dissolved in acetone and filtered over 0.45 mm PTFE filters (4 mm; BGB, USA).

173 **3.5 Ladderane analysis**

174 A commercially available deuterated $C_{20}[5]$-PUFA (Reagecon Diagnostics Ltd.) was added as an internal standard to the

175 FAME fractions. FAME fractions were analysed on an Agilent 1290 Infinity I ultra-high performance liquid

176 chromatographer (UHPLC), equipped with a thermostatted auto-injector and column oven, coupled to a Q Exactive Plus

177 Orbitrap MS, with an atmospheric pressure chemical ionization (APCI) probe (Thermo Fischer Scientific, Waltham, MA)

178 operated in positive ion mode. Separation was achieved with a ZORBAX Eclipse XDB C_{18} column (Agilent, 3.0×250 mm,

179 5 μm), using MeOH as an eluant (0.4 ml min^{-1}). APCI source settings were set as follows: corona discharge current, 2.5 μA;

180 source CID, 10 eV; vaporizer temperature, 475°C; sheath gas flow rate, 50 arbitrary units (AU); auxiliary gas flow rate,

181 30AU; capillary temperature, 300°C; and S-lens, 50V (van Kemenade et al., 2022). A mass range of *m/z* 225–380 was

182 monitored (resolution 140,000 ppm), followed by data-dependent MS^2 (resolution 17,500 ppm at *m/z* 200), in which the 10

183 most abundant masses in the mass spectrum were fragmented successively (stepped normalised collision energy 20, 25, 30).

184 An inclusion list containing the exact masses of C_{14-24}-[3]- and C_{14-24}-[5]-ladderane FAMEs was used. Mass chromatograms

185 (within 5 ppm mass accuracy) of the protonated molecules ([M+H]$^+$) were used to integrate the detected ladderanes: $C_{14}[3]$-,

186 $C_{14}[5]$, $C_{16}[5]$, $C_{18}[3]$-, $C_{18}[5]$-, $C_{20}[3]$- and $C_{20}[5]$-ladderane FAMEs (*m/z* 235.169, 233.154, 261.185, 291.232, 289.216,

319.263 and 317.248, respectively), and the internal deuterated $C_{20}[5]$-PUFA standard (m/z 322.279). A detection limit of 30–35 pg injected on-column and a linear response of ($r(4) > 0.99$) over approximately 3 orders of magnitude was achieved (S1, Table 8a). Identification of ladderanes was achieved by comparing retention times and spectra with in-house isolated $C_{20}[3]$- and $C_{20}[5]$-ladderane FAME standards (Hopmans et al., 2006; Rattray et al., 2008) and with ladderane FAMEs in a biomass sample of *Ca.* Kuenenia.

Previously, ladderane FAME quantification has been conducted using calibration curves of in-house isolated $C_{20}[3]$- and [5]-ladderane standard (Hopmans et al., 2006). However, this quantification method does not correct for any variability in ion intensity, due to e.g., matrix effects and/or changes in the instruments functioning. Therefore, we further optimised this quantification method to include a response correction using a commercially available internal standard (deuterated $C_{20}[5]$-PUFA). At the start of each sequence, calibration curves were made for the $C_{20}[3]$- and [5]-ladderane standards *and* the deuterated $C_{20}[5]$-PUFA standard. The relative response of the deuterated $C_{20}[5]$-PUFA commercial standard in relation to the ladderane FAME standards was determined from the slopes of their calibration curves (giving a relative response factor, i.e. RRF). An RRF of 1.3 was used for [3]-ladderanes, based on the $C_{20}[3]$-ladderane, and an RRF of 1.2 for the [5]-ladderane, based on the $C_{20}[5]$-ladderane. Using the RRFs, ladderane FAME concentrations (C_L, expressed in µg · g dry weight^{-1}) were calculated as follows:

$$C_L = \frac{m_{IS}\left(\frac{A_L}{\left(\frac{A_{IS}}{RRF}\right)}\right)}{m_S} \qquad [1]$$

With m_{IS} being the mass (µg) of the added internal standard, m_S the dry weigh of extracted sediment (g), A_L the integrated peak area of the given ladderane FAME , A_{IS} the integrated peak area of the internal standard, and RRF the relative response factor. Ladderane concentrations (including concentrations normalized against gram TOC) are reported in supplement 1 (Tables 4 and 5). To compare with previous studies that did not use an internal standard, the established method that uses external calibration curves of three authentic standards (Hopmans et al., 2006; Rush et al., 2012b; Rattray et al., 2010) was also performed (S1, Table 8b; S2.2). A comparison between both quantification methods is provided in supplementary material 2 (sect. S2.2).

3.6 NL$_5$ index

The index of ladderane lipids with five cyclobutane rings (NL$_5$) correlates with the temperature at which they were synthesised. The NL$_5$ index is calculated according to the following equation:

$$NL_5 = \frac{C_{20}[5]ladderane\ FA}{C_{18}[5]ladderane\ FA + C_{20}[5]ladderane\ FA} \qquad [2]$$

214   The empirical fourth-order sigmoidal relationship between the NL_5 index and temperature is then described by:

215
$$NL_5 = 0.2 + \frac{0.7}{1 + e^{-(\frac{T-16.3}{1.5})}}$$
[3]

216   with temperature (T) in °C (Rattray et al., 2010).

3.7 Degradation rates and constants

218   Ladderane concentrations over the entire record (Fig. 3) were used to calculate ladderane degradation rates, with the

219   following equation for lipid degradation (Canuel and Martens, 1996):

220
$$k' = \frac{-\ln[\frac{C_t}{C_{t0}}]}{t}$$
[4]

221   With k' being the first order rate constant (kyr^{-1}), C being the concentration (µg g sediment^{-1}) at time t (C_t) and at the initial

222   time (C_{t0}), and t being the relative time (kyr). Ladderane degradation constants and rates are provided in supplementary

223   material 1 (Table 7).

4 Results

4.1 Bulk sedimentary total nitrogen and total organic carbon

226   Bulk sedimentary total nitrogen (TN) ranged between 0.1–0.6 % throughout the record. $\delta^{15}N$ fluctuated from 5.8 to 10.0 ‰.

227   An offset of 3 to 4 ‰ was observed between interglacials and glacials, with higher values during interglacials. Sedimentary

228   total organic carbon (TOC) varied between 1.7–7.4 % throughout the record, whilst its carbon isotopic composition

229   ($\delta^{13}C_{TOC}$) ranged from -23.0 to -21.6 ‰. C/N ratios (atomic) ranged from 13 to 23 (Fig. 4F–J; S1, Table 3).

4.2 Ladderane FAs concentrations & the NL$_5$ index

231   The ladderane fatty acids identified in this record were $C_{18}[5]$-, $C_{18}[3]$-, $C_{20}[5]$- and $C_{20}[3]$-ladderanes and their diagenetic

232   products, the SC $C_{14}[5]$-, $C_{14}[3]$- and $C_{16}[5]$-ladderanes. Summed SC-ladderane and ladderane concentrations over the entire

233   500 ka record were 0.5–33 and 0.1–23 ng g^{-1} dry weight, respectively (Fig. 3; S1 Table 5). Normalized concentrations over

234   the 160 ka record ranged as follows: $C_{14}[5]$-ladderane 16–158 ng gTOC^{-1}, $C_{14}[3]$-ladderane 27–184 ng gTOC^{-1}, $C_{16}[5]$-

235   ladderane 34–198 ng gTOC^{-1}, $C_{18}[5]$-ladderane 7–107 ng gTOC^{-1}, $C_{18}[3]$-ladderane 4–76 ng gTOC^{-1}, $C_{20}[5]$-ladderane 5–79

236   ng gTOC^{-1}, and $C_{20}[3]$-ladderane 10–208 ng gTOC^{-1} (Fig. 4B, C; S1, Table 4). Concentrations calculated without the use of

237   the internal standard (Hopmans et al., 2006; see sect. 2.5) are reported in S1 (Table 8b) and were a factor 1.2 and 1.3 lower

238   for [3]-(SC-)ladderanes [5]-(SC-)ladderanes, respectively. Concentrations calculated with the two quantification methods

239 showed a strong positive linear relationship of $R^2 = 0.88$ and 0.89 for [3]-(SC-)ladderanes and [5]-(SC-)ladderanes,

240 respectively (Fig. S2). The NL_5 index (eq. [2]) ranged from 0.3 to 0.8 throughout the record. Corresponding NL_5-derived

241 temperatures (eq. [3]) were between 13.1–18.6°C, with highest values observed in >160 cal ka BP sediments (S1, Table 6).

242
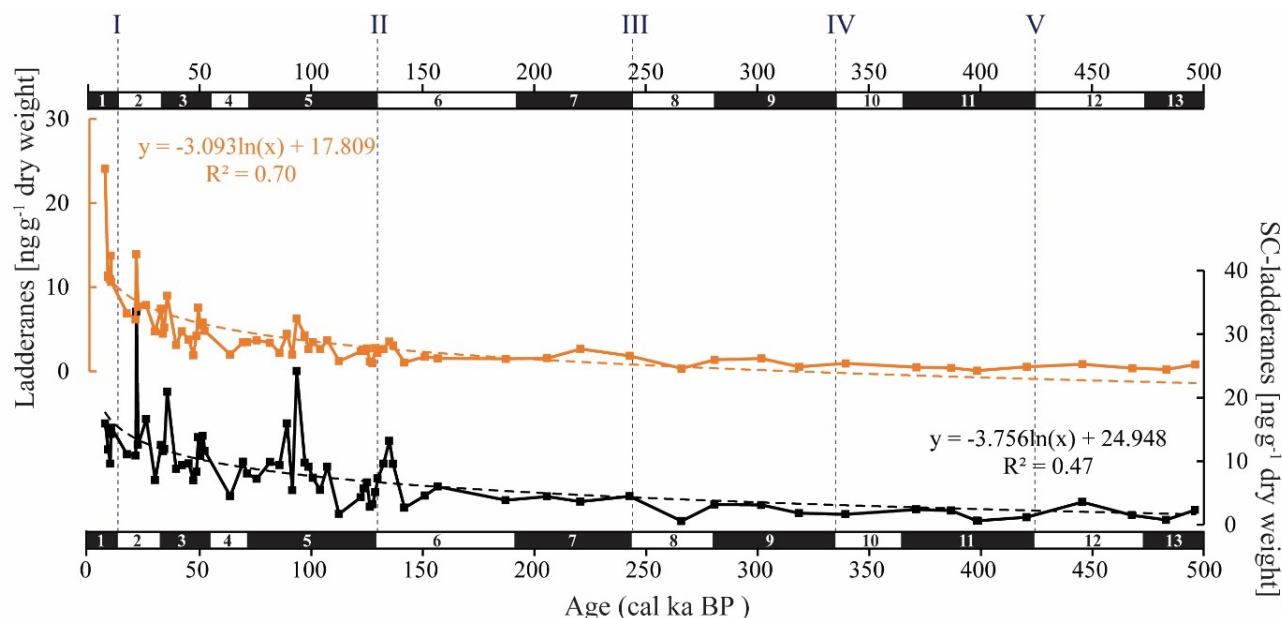
Figure 3: Summed C_{18}[5]-, C_{18}[3]-, C_{20}[5]- and C_{20}[3]-ladderane (orange) and summed short-chain (SC) C_{14}[5]-, C_{14}[3]- and C_{16}[5]-ladderane (black) concentrations (ng g^{-1} dry weight) in the ODP 1012 record. The logarithmic relationship between ladderanes and SC-ladderanes with time is provided (with corresponding R^2), and displayed with orange and black spaced lines, respectively. Grey spaced lines indicate the approximate timing of glacial terminations I to V. N.B. the scales of the y-axes are different.

247 **5 Discussion**

248 In the sediment record of ODP site 1012, C_{18}[3]-, C_{18}[5]-, C_{20}[3]- and C_{20}[5]-ladderane FAs and their short chain C_{14}[3]-,

249 C_{14}[5]-, C_{16}[5]-products were detected over the last 500 kyr (~38 mbsf; Fig. 3). This poses a considerable extension of the

250 ladderane record (formerly detected up to ~140 ka BP in Arabian Sea sediments; ~10 mbsf; Jaeschke et al., 2009). Below,

251 we will first discuss the provenance of the detected ladderane lipids (sect. 5.1). Then, their variability throughout glacial-

252 interglacial cycling (sect. 5.2), ending with the subsequent implications on our understanding of the nitrogen cycle of the

253 CCS (sect. 5.3). Unfortunately, the coarse sampling resolution in >160 cal ka BP sediments and low ladderane FA

254 concentrations (due to diagenesis) complicate interpretations of ladderane FA fluctuations in these sediments. Therefore,

255 analysis of trends in ladderane concentrations over (inter)glacial cycling is limited to <160 cal ka BP sediments.

256 **5.1 Ladderanes sourced from anammox bacteria in the ESTNP OMZ water column**

257 The relative contribution of SC-ladderanes to the total ladderane pool is a measure of oxygen exposure (Rush et al., 2011,

258 2012b), and the NL_5-index is a measure of the water temperature of the niche of anammox bacteria (Rattray et al., 2010). In

259   combination, these data may provide insights into the origin of ladderanes in the CCS sediment record.

260
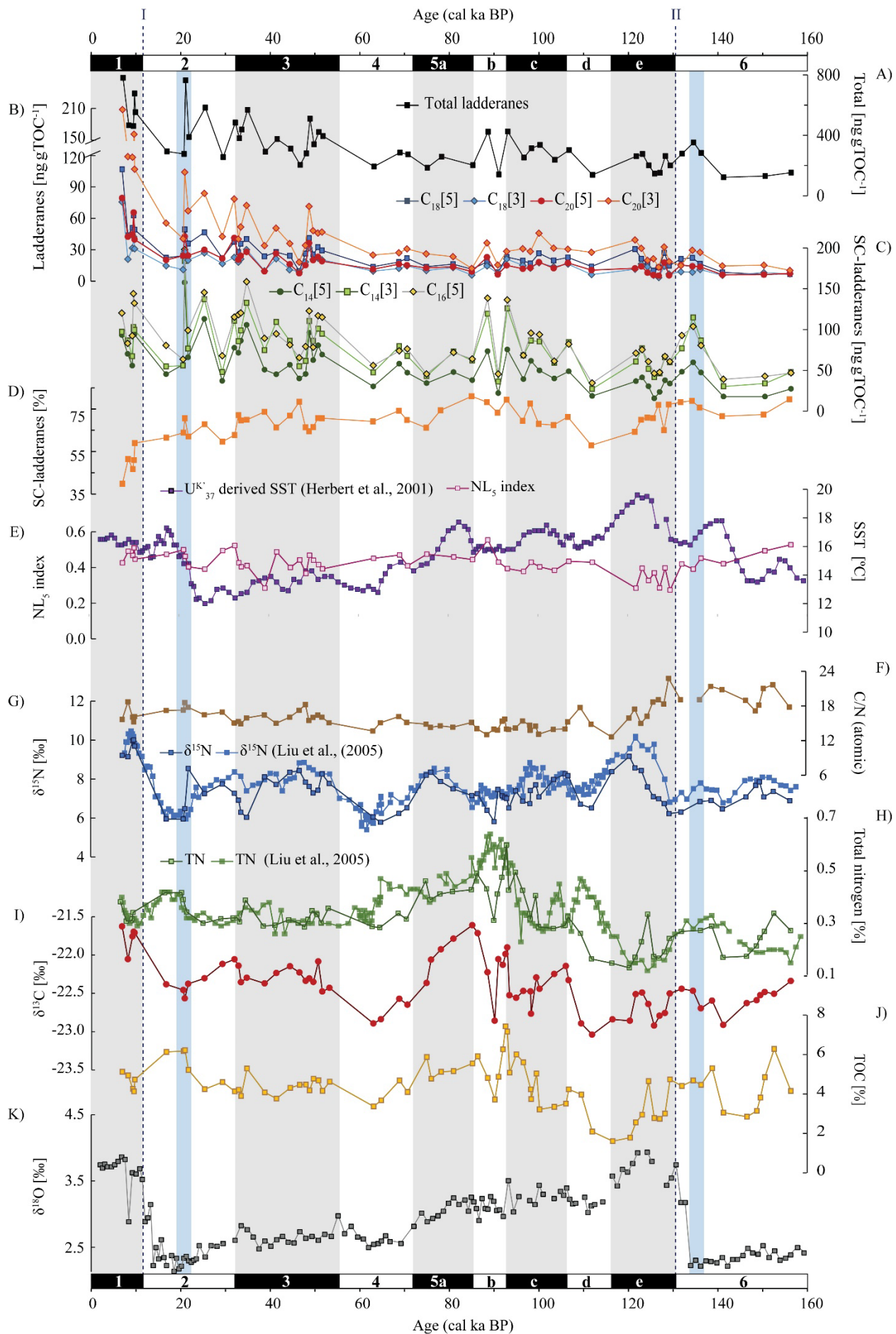
 Figure 4: From top to bottom: concentrations of A) total ladderanes (summed SC-ladderanes and ladderanes), B) ladderanes and C) SC-

262 ladderanes (normalized against TOC [ng gTOC^{-1}]), D) relative abundance of SC-ladderanes over total ladderanes [%], E) $U^{K'}_{37}$ derived

263 sea-surface temperatures (SST) from Herbert et al., (2001) [°C] and the NL$_5$-index from this study, F) atomic ratio of total organic carbon

264 (TOC) over total nitrogen (TN), G) bulk sedimentary δ^{15}N from Liu et al., (2005) and this study [‰], H) TN from Liu et al., (2005) and

265 this study [%], I) bulk sedimentary δ^{13}C [‰], J) TOC [%] and K) benthic δ^{18}O record from Herbert et al., (2001) [‰]. All data is derived

266 from the same location (ODP site 1012). Marine isotope stages (MIS) are indicated with black and white bars. Periods of maximum global

267 ice volume (Herbert et al., 2001; blue bars) and the approximate timing of glacial terminations TI and TII (dashed lines) are also indicated.

268   In the CCS, a progressive depletion of both the water column $\delta^{15}N_{NO3}$ and sedimentary δ^{15}N signal occurs with

269 increasing latitude, resulting in more depleted values at ODP site 1012 (8–10 ‰; Altabet et al., 1999; Liu et al., 2005; this

270 study) than in the ETNP OMZ core. The northward transport of denitrified waters by the poleward flowing oxygen-poor CU

271 from the core of the ETNP has been evoked to explain this trend. (Castro et al., 2001; Kienast et al., 2002). This means that

272 at ODP site 1012, the sedimentary δ^{15}N signal is thought to predominantly derive from the ETNP, and not the ESTNP OMZ.

273 In order to understand the observed ladderane trends in the ODP site 1012 record, it is thus important to establish whether

274 the detected ladderanes reflect a local signal (from the ESTNP OMZ) or whether they are also sourced from the ETNP OMZ

275 core and similarly transported northwards with the CU, towards ODP site 1012. Alternatively, ladderanes could also be

276 synthesized by sedimentary anammox bacteria (Vossenberg et al., 2008).

277   At ODP site 1012, SC-ladderanes were present at relative abundances of 40–88 % throughout the record (Fig. 4D).

278 Ladderane FAs are relatively labile compounds, and in the Arabian Sea have been shown to already degrade into their SC-

279 products (at relative proportions of ~20 %) within the OMZ water column (DO <3 µmol L^{-1}). There, the sinking of

280 ladderanes through the oxygenated bottom waters underlying the OMZ ultimately resulted in similar relative abundances of

281 SC-ladderanes in the surface sediments of 20–80 %, depending on water column depth (Rush et al., 2012b). The similarly

282 high contribution of SC-ladderanes in the ODP 1012 record suggest ladderanes are also sourced from an overlying OMZ

283 water column (i.e. the ESTNP OMZ) and sunk through oxygenated bottom waters before being deposited on the seafloor,

284 which readily became anoxic in view of the high TOC content (Fig. 4J).

285   An OMZ water column source is consistent with the NL$_5$ index (0.3–0.8; Fig. 4E). According to the NL$_5$-calibration

286 by Rattray et al., (2010), NL$_5$ indices within this range more closely reflect water column rather than sedimentary anammox

287 bacteria. Also, NL$_5$-derived temperatures (13–17°C; S1, Table 6) are significantly higher than what would be expected for

288 sea-floor temperatures (i.e., modern annual average bottom water temperatures at site 1012 are <5°C; WOA, 2018).

289 Additionally, while the transport of ladderane FAs has been shown to occur within oxygen-depleted systems (van Kemenade

290 et al., 2022), long-distance transport of ladderane FAs with the CU (characteristic DO concentration of ~62 µmol L^{-1} in

291 modern CU water; Sahu et al., 2022) is unlikely, and would be expected to yield higher relative abundances of SC-ladderane

FAs than detected in the record. Transport of ladderanes is also not reflected in present-day ENP ladderane distributions, as an investigation of ladderanes at a more northerly (~20°N) and a more southerly (~17°N) located site showed *in situ* synthesis by pelagic *Ca.* Scalindua at both sites (Sollai et al., 2015). Hence, ladderane FAs are thought to predominantly derive from the ESTNP OMZ water column and reflect a local anammox signal, although some contribution of allochthonous or sedimentary anammox cannot be entirely excluded.

5.2 Anammox variability in the CCS over the last 160 kyr

5.2.1 The Holocene and MIS-5, including the penultimate interglacial of MIS 5e

Over the ~500 cal ka BP record, ladderane FAs are observed to decrease logarithmically with time (Fig. 3; $R^2 = 0.70$), in which the degradation constant k follows a linear relationship (when logarithmically transformed; Fig. 5A; $R^2 = 0.88$) with time. This is consistent with first order degradation kinetics, typical for OM (Canuel and Martens, 1996). As such, it is not surprising that the highest ladderane concentrations are observed in the youngest sediments, deposited during the early to mid-Holocene. Even so, ladderane FAs normalized against TOC also show elevated concentrations in Holocene sediments. This suggests high ladderane FAs at this time are not simply a preservation signal but also reflect an increase (compared to pre-Holocene sediments) in their production by *Ca.* Scalindua spp. relative to the total organic C pool. Moreover, elevated ladderanes in early to mid-Holocene sediments coincide with enriched bulk $\delta^{15}N$ (9–10 ‰; Fig. 4G), indicative of enhanced N-loss by anaerobic microorganisms, and elevated TOC and TN concentrations (Fig. 4H, J), indicative of increased productivity.

In contrast to ladderane FAs, concentrations of their SC-products are not highest in Holocene sediments. Consequently, the SC-ladderane data does not fit the logarithmic decrease with time well ($R^2 = 0.47$; Fig. 3), which is also reflected in the relationship of the degradation constant k with time (Fig. 5A; $R^2 = 0.43$). The oxidation of ladderane FAs to produce SC-ladderane FAs (Rush et al., 2011) has been shown to take place within the oxic waters below the OMZ. In this way, 20–80 % of the ladderane FAs were transformed into SC-ladderanes in the Arabian Sea (Rush et al., 2012c). Throughout the deeper CCS sedimentary record (>10 cal ka BP), the relationship between ladderane FAs and their SC-products follows a linear trend ($R^2 = 0.87$; Fig. 5B), with SC-ladderanes making ~60–80 % of total ladderanes (Fig. 4D). However, in Holocene sediments (<10 cal ka BP sediments), the relationship between ladderanes and SC-ladderanes is different (Fig. 5B), and SC-ladderanes occur at relatively lower abundance (40– 60 %) compared to the rest of the record. This indicates that after 10 cal ka BP, there was no significant change in the exposure of ladderane FAs to the oxygenated water underlying the ETNP OMZ before being buried in the sediment record, but that in the recent record, there was reduced oxygen exposure.

Reduced oxygen exposure is likely to have resulted from an intensified OMZ; Lembke-Jene et al. (2018) showed, using palaeoceanographic proxies and palaeomodeling, that a combination of sea ice loss, increased SST and remineralization rates led to more deoxygenated intermediate waters (the NPIW) during the early to mid-Holocene in the North Pacific. Moreover, in the ETNP, enriched sedimentary $\delta^{15}N$ values and laminated sediments during the early Holocene, alongside geochemical tracers, have been interpreted to signal the presence of a strong OMZ at this time, while bioturbated sediments occurred over the last glacial period (Thunell and Kepple, 2004).

Ladderane FAs concentrations also peak during the penultimate interglacial (the Eemian; MIS 5e), in line with enriched (>8 ‰) $\delta^{15}N$ values. Microfossil data from MIS 5 has indicated that intermediate waters in the western North Pacific were more deoxygenated during the Eemian (Matul et al., 2016), which may have driven increased anammox in the CCS at this time. Yet, while $\delta^{15}N$ values over MIS 5 maximize during MIS 5e, ladderane FAs concentrations peak during mid-MIS 5 (MIS 5b–c). During MIS 5b–d, when (SC-)ladderane FA concentrations maximize, intermediate waters in the western North Pacific were likely oxic (Matul et al., 2016) and the $\delta^{15}N$ signal is more subdued (<8 ‰; Fig. 4G). At this time, increased (SC-)ladderane FAs coincide with peaks in paleo-productivity proxies (i.e., TOC and TN; Fig. 4H, J). Over the course of MIS 5, from late MIS 5e onwards, SSTs in the CCS decreased while the CC strengthened (Herbert et al., 2001; Yamamoto et al., 2007). This would have led to increased transport of high-oxygen, nutrient-rich NPIW (Herguera et al., 2010) and enhanced open ocean upwelling. This may have fuelled productivity, which explains the high TOC and TN concentrations in mid-MIS 5.

The C/N ratio remains fairly stable throughout MIS 1 to MIS 5c (MN = 16, STD = 2); Fig. 4F), with higher values observed during MIS 6 (MN = 20, STD = 2; discussed in sect. 5.2.2). Based on stoichiometry, enhanced NO_3^- supply is expected to lower the ratio in phytoplankton biomass (Matsumoto et al., 2020). Yet, changes in nutrient concentrations have been observed to effect the C/P and N/P, but not the C/N ratio (Frigstad et al., 2011). It is therefore not surprising that the increased TN content during mid-MIS 5 is not reflected in the C/N ratio. Also, while the $\delta^{13}C$ signal (-23 to -22 ‰; Fig. 4I) reflects a typical marine origin of OM, the C/N ratio is higher than commonly observed for marine algae (e.g., Lamb et al., 2006). This is likely caused by preferential remineralization of organic N during the settling of OM from the photic zone (Verardo & Mcintyre, 1994; Schneider et al., 2003).

During mid-MIS 5, where TN and TOC peak, anammox may have been fuelled by local increases in OM. Babbin et al., (2014) showed, using incubations from the ETNP OMZ, that anammox rates increase in response to the addition of OM. Likewise, in the modern Southern Pacific OMZ, N-loss by anammox was found to be strongly correlated with the export of OM, via the release of ammonium into the water column through remineralization (Kalvelage et al., 2013). As such, the co-occurrence of ladderane FA and paleo-productivity proxies maxima during MIS 5, could reflect an increase in *Ca.* Scalindua

351   spp. abundance in response to an increased N-substrate supply via OM-remineralization or nutrient transport.

352   Remineralization of increased phytoplankton biomass may consequently also have led to more reduced local conditions,

353   which would also favour anammox. This local signal would not have been recorded in the western part of the North Pacific,

354   where intermediate waters were oxic (Matul et al., 2016) . The relatively subdued δ^{15}N signal during mid-MIS 5, and

355   consequent implications for our understanding of the N-cycle in the CCS are further discussed in sect. 5.3.
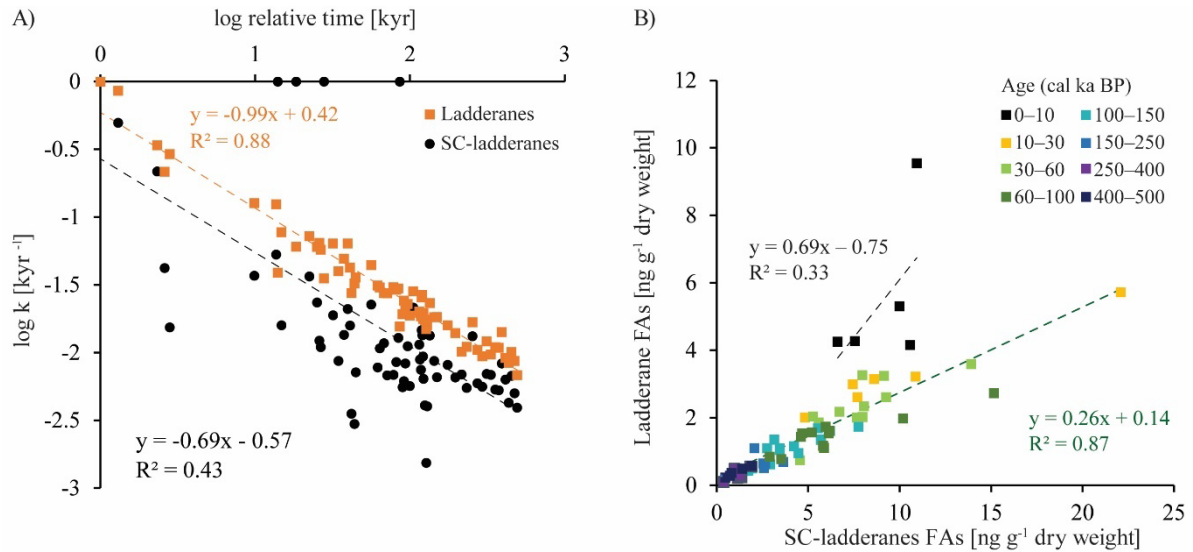
356

357   **Figure 5:** A) Linear relationship between the logarithmic values of the degradation constant k and relative time for ladderane FAs (orange

358   squares) and SC-ladderane FAs (black dots). B) Relationship between ladderane FAs and SC-ladderane FAs, in which samples are colour-

359   coded according to age. The linear relationship and corresponding R^2 are given for the most recent age group (0-10 cal ka BP; in black)

360   and the >10 cal ka BP age groups (in green).

361   **5.2.2 The two most recent glacial periods**

362   Ladderane FAs are observed to increase from early MIS 3 to mid-MIS 2, and from mid- to late-MIS 6. Maxima of

363   ladderanes occur approximately at the timing of icesheet volume maxima of the last glacial maxima (LGM) and the

364   penultimate glacial of MIS 6 (blue bars in Fig. 4; following timing of Herbert et al., 2001). During the last glacial period

365   (~115–12 ka BP) and the penultimate glacial MIS 6, large parts of the North American continent were covered by the

366   Laurentide and Cordilleran ice sheets. While glacials are typically associated with a well-ventilated intermediate-water mass

367   (Herguera et al., 2010) and a strong southward advection of the CC (Ortiz et al., 1997), a weakening of the CC has been

368   proposed to occur at times of global ice sheet maxima. In the CCS, $U^{K'}_{37}$-derived temperatures indicate that SSTs increased

369   ~12 kyr in advance of maximal ice-sheet volumes. This is thought to reflect increased northward advection of warm oxygen-

370   poor waters carried by the CU and DC in response to a weakened CC due to large ice-sheet volumes (Herbert et al., 2001).

371   Using trace elements, Cartapanis et al., (2011) found that intermediate water oxygenation off Baja California deteriorated

372   slightly over the course of late MIS 3 and early MIS 2, consistent with a strengthening of the CU at this time. As such, the

373 increased abundance of ladderanes observed during (and leading up to) ice sheet maxima at ODP site 1012, may derive from

374 an increased *Ca.* Scalindua spp. abundance due to more reduced local conditions, via the enhanced strength of the CU.

375 MIS 6 and its termination (T2) are further characterized by relatively high C/N ratios (17–23; Fig. 4F). Matsumoto

376 et al., (2020) found, using a global ocean carbon cycle model, that during glacial periods the expansion of sea ice increased

377 global C:N:P ratios. Additionally, taxonomic changes during glacials, in which eukaryotic phytoplankton became more

378 dominant, resulted in NO_3^- depletion (hereby increasing the C/N ratio). At the same time, decreased upwelling during glacial

379 periods in the North Pacific (Worne et al., 2019) may have also lowered nutrient availability. Low N-availability is reflected

380 in relatively low TN concentrations in this record (Fig. 4H). This suggests anammox at this time was primarily promoted by

381 reduced local DO concentrations via enhanced CU strength, rather than enhanced nutrient supply and/or increased

382 remineralization rates.

383 While enhanced anammox in response to deoxygenation during glacial maxima is at odds with previous

384 assessments of N-loss in the CCS (e.g., Liu et al., 2005), deoxygenation of the Pacific is consistent with recent paleo-proxy

385 studies (Lu et al., 2016; Anderson et al., 2019) and modelling results (Matsumoto et al., 2020). According to these studies,

386 many parts of the glacial ocean, including the equatorial Pacific, had substantially lower DO during the last glacial period

387 than today. This fits with increased ladderane FAs at this time, which suggests N-loss in the CCS was likely more intense

388 during glacial maxima than previously assumed.

389 **5.3 Implications of the occurrence of anammox on the N cycle in the CCS**

390 In the CCS, previous estimates of changes in N-loss over time have been based on the bulk sedimentary $\delta^{15}N$ record.

391 Enriched $\delta^{15}N$ during interglacials (7–10 %) are thought to reflect intensified denitrification in response to reduced DO,

392 while more depleted $\delta^{15}N$ during glacials (4–6 %) are assumed to reflect lowered rates in response to increased DO (Liu et

393 al., 2005; 2008). However, the occurrence of ladderane FAs throughout our CCS record now shows that anammox was (also)

394 responsible for N-loss and thus contributed, at least partially, to the sedimentary $\delta^{15}N$ record.

395 The cross-correlation for both $\delta^{15}N$–$\delta^{18}O$ and $\delta^{18}O$–SST at ODP site 1012 (Liu et al., 2005) indicates that

396 fluctuations in $\delta^{15}N$ occur in tandem with glacial-interglacial cycling. However, a long-standing conundrum has been the

397 discrepancy between the $\delta^{15}N$ record and productivity proxies (i.e., TOC and TN), especially north of the ETNP (Kienast et

398 al., 2002), as also seen in our record (Fig. 4). This decoupling has been used previously to suggest that variations in

399 denitrification was not due to changes in OM remineralization rate, but rather from changes in ocean circulation and

400 ventilation patterns (Ganeshram et al., 2000). Yet, fluctuations in ladderanes *do* seem to follow trends in paleo-productivity

401 proxies (i.e., TOC and TN) relatively closely, especially during the Holocene, MIS 3 and MIS 5. And, while enriched $\delta^{15}N$

402 values sometimes correspond to ladderane maxima (i.e. during the Holocene), discrepancies with ladderane concentrations

403 are seen especially during MIS 5, and during glacial periods (Fig. 4).

404   This may suggest that increased anammox does not always correspond to increased N-loss, possibly via

405 simultaneously reduced denitrification rates (Koeve and Kähler, 2010). Yet, Babbin et al., (2014) showed, using incubations

406 from the ETNP OMZ, that both denitrification and anammox are limited by OM supply, and their rates increase in response

407 to the addition of OM. Moreover, these authors showed that both denitrifiers and anammox bacteria are similarly inhibited

408 by oxygen in the marine environment, at DO concentration around 3 to 8 μmol L^{-1} (Babbin et al., 2014). As such, both

409 anammox and denitrification should respond similarly to changes in DO and OM in the CCS.

410   Moreover, given the average C/N signature of marine OM (106:16; Redfield, 1963), stoichiometric constraints

411 should result in a ratio of N_2 production via denitrification and anammox of 71:29 (Koeve and Kähler, 2010). On the one

412 hand, this means that the relative contribution of anammox to N_2-production is likely lower than the contribution of

413 denitrification, possibly resulting in a less strong influence of anammox on the $\delta^{15}N$ signal. On the other hand, this means

414 that denitrification and anammox rates should be positively related, in which increased anammox is associated with

415 increased denitrification (Koeve and Kähler, 2010). Potentially, anammox and denitrification could be unsynchronized (as

416 indicated by differences between the ladderane and $\delta^{15}N$ records) in response to variations in the C/N ratio of OM. Localized

417 variations in the C/N signature may result in different relative contributions. Yet, integrating these variations over space and

418 time should obtain a similar ratio (Dalsgaard et al., 2012; Babbin et al., 2014; Ward, 2013). Additionally, the C/N ratio

419 remains fairly consistent throughout the record (13–19), except during MIS 6 where it is higher (17–23; Fig. 4F) and

420 variations do not correspond to those observed in ladderane FAs or $\delta^{15}N$. As such, given the temporal resolution of the

421 record (which does not cover seasonality), denitrification and anammox intensities are expected to fluctuate in-tandem.

422   Consequently, variability in $\delta^{15}N$ of the CCS sedimentary record may, at times, simply not relate directly to changes

423 in denitrification and/or anammox rates. Reconstructions of N-loss using sedimentary $\delta^{15}N$ depend on the assumption that

424 there was complete biological utilization of NO_3^- by phytoplankton. However, during periods of high upwelling intensity (as

425 likely occurred during mid-MIS 5; see sect. 5.2.1), the high NO_3^- availability may result in incomplete NO_3^- assimilation.

426 This allows for the preferential uptake of ^{14}N by primary producers, resulting in a pool of $\delta^{15}N$ depleted OM available for

427 heterotrophic denitrification (Tesdal et al., 2013). Hence, at times of high NO_3^- supply, incomplete nitrate assimilation

428 would have quenched the $\delta^{15}N$ signal, even if denitrification was as intense as during periods of low NO_3^- availability.

429 Moreover, a study by Altabet and Francois (1994) showed that sedimentary $\delta^{15}N$ in the equatorial Pacific records the

430 isotopic enrichment of near-surface NO_3^- via depletion by phytoplankton, in which enriched $\delta^{15}N$ values are associated with

431 reduced NO_3 availability for phytoplankton assimilation. Also, in the South Pacific, NO_3^- concentrations have been found to

432 affect the $U^{K'}_{37}$ index (Placencia et al., 2010). Given the phase-relationship between the $\delta^{15}N$ and $U^{K'}_{37}$ -based SST records

433 of the CCS (Liu et al., 2008) and the discrepancies between the $\delta^{15}N$ and ladderane records, it may be reasonable to conclude

434 that the CCS sedimentary $\delta^{15}N$ fluctuations (also) record variations in NO_3^- assimilation by phytoplankton.

435   Additionally, other biological processes may influence the $\delta^{15}N$ signal (Zonneveld et al., 2010). In the Gulf of

436 Tehuantepec, at the southern end of the ETNP OMZ core, $\delta^{15}N$ values decrease over the course of the Holocene (Thunell and

437 Kepple, 2004; Hendy and Pedersen, 2006), while laminated sediments suggest reduced DO concentrations. This was

438 interpreted as being the result of increased N_2-fixation ($\varepsilon: \leq +2$ ‰; Sigman and Fripiat, 2019), which lowered the

439 "denitrification" $\delta^{15}N$ signal (Thunell and Kepple, 2004). Lastly, enrichment of the sedimentary $\delta^{15}N$ values occurs during

440 early burial, where oxygen exposure results in enhanced biological isotopic alteration (Robinson et al., 2012). In short,

441 sedimentary $\delta^{15}N$ is shaped by many opposing processes, and assuming a one-on-one relationship with denitrification

442 intensities and DO concentration clearly misses the complexity that shape the CC system. Ladderanes hereby offer a more

443 detailed picture of N-loss dynamics in the paleoenvironment of the CCS. In the case of the ODP site 1012 record, ladderane

444 concentration trends challenge the conventional assumption that N-loss processes solely follow ocean circulation and

445 ventilation patterns coupled to (inter)glacial cycling, and instead show OM remineralization may also be an important driver

446 of N-loss.

447   Discrepancies between the ladderane and $\delta^{15}N$-record hereby necessitate careful consideration when applying N-

448 isotope based budgets to estimate past N-cycling. More specifically, the occurrence of increased ladderane concentrations

449 during glacial maxima may require a re-evaluation on the response of N-loss rates to glacial-interglacial cycling in the CCS.

450 Furthermore, the occurrence of an additional N-loss pathway in the CCS (anammox), other than denitrification, may affect

451 estimates of N_2O greenhouse-gas production by denitrifiers and the degree of heterotrophy of the system, although the

452 importance of this would require further investigation. Future research, investigating anammox biomarkers in other CCS

453 records (preferably in a latitudinal gradient with this record) may offer further insights into N-loss dynamics across glacial-

454 interglacial cycles.

455 **6 Conclusion**

456 Ladderane FAs detected in a ~500 kyr CCS sedimentary record at ODP site 1012 reveal the past occurrence of anaerobic

457 ammonium oxidising (anammox) bacteria in the water column of the California current system (CCS) over the last five

458 glacial terminations. The index of ladderanes with five cyclobutene moieties (NL_5), which correlates with the *in situ*

459 temperature at which ladderanes are synthesised, suggests that ladderanes were derived from the ETSNP OMZ water

460 column. The CCS record shows a continuous presence of ladderane FAs over the last two interglacial-glacial transitions,

461 with maxima during: i) the Holocene, ii) leading up to and during the LGM (early MIS 3 to mid-MIS 2), iii) MIS 5b-c and

462 iv) during the ice sheet maxima of the penultimate glacial (late MIS 6). Combining information on the presence of

463 ladderanes with paleo-productivity proxies and the hydrographic features of the CCS suggests anammox abundance was

464 driven both by OM-remineralization and advection changes, which regulated nutrient and oxygen concentrations. In the

465 record, a clear shift is seen in the relationship of SC-ladderanes over their parent products, in which the relative abundance of

466 SC-ladderanes is significantly lower in Holocene than in pre-Holocene sediments. This may reflect a shift in oxygen

467 exposure, which corresponds to previous studies showcasing a vertical expansion of the ENP OMZ over the Holocene.

468 Clearly, the anammox contribution to N-loss in the CCS, as shown in this study, requires a reassessment of biogeochemical

469 cycling in this system. Discrepancies between the ladderane and $\delta^{15}N$ record may imply that N-loss was perhaps more

470 intense during cold phases than previously assumed. Careful considerations must thus be taken when using N-isotope based

471 budgets to estimate past N-cycling in the CCS; sedimentary $\delta^{15}N$ is shaped by many opposing processes, and assuming a

472 one-to-one relationship between N-loss intensities and OMZ variability clearly overlooks the complexity that shapes the CC

473 system. Ladderanes hereby offer a more holistic picture of N-loss dynamics in the paleoenvironment of the CCS.

474 **Data availability.** All data discussed in this paper is available in the supplementary material 1. Data from supplementary

475 material 1 can be retrieved via the following doi: 10.25850/nioz/7b.b.sg

476 **Supplement.** The supplement related to this article is available on-line at:

477 **Author contributions.** ZE and ZRvK performed the laboratory work. ZRvK conducted the data analysis and writing of the

478 manuscript. ZE created the age-model. ECH developed and optimized the UHPLC-HRMS method for the analysis of

479 ladderane lipids. DR provided the supervision of the project. DR, ZE and ZRvK designed and conceptualized the project.

480 JSDD provided critical support in data interpretation. All authors contributed to the writing of the manuscript.

481 **Competing interests.** The authors declare that they have no conflict of interest.

482 **Acknowledgements.** We thank the captain and crew of Ocean Drilling Program Leg 167 for the collection of all sampled

483 material used in this study. Denise Dorhout and Monique Verweij are also greatly appreciated for their support with the

484 instrumental analysis. We also kindly thank Ronald van Bommel and Marcel van der Meer for their help in the isotope lab.

485 **Financial support.** This research was supported by the Soehngen Institute of Anaerobic Microbiology (SIAM) Gravitation

486 Grant (024.002.002), awarded to JSSD by the Dutch Ministry of Education, Culture and Science (OCW).

487 **References.**

488 Altabet, M. A. and Francois, R.: Sedimentary nitrogen isotopic ratio as a recorder for surface ocean nitrate utilization, Global

489 Biogeochem Cycles, 8, 103–116, https://doi.org/10.1029/93GB03396, 1994.

490   Altabet, M. A., Pilskaln, C., Thunell, R., Pride, C., Sigman, D., Chavez, F., and Francois, R.: The nitrogen isotope

491   biogeochemistry of sinking particles from the margin of the eastern North Pacific, Deep Sea Res 1 Oceanogr Res Pap, 46,

492   655–679, https://doi.org/10.1016/S0967-0637(98)00084-3, 1999.

493   Anderson, R. F., Sachs, J. P., Fleisher, M. Q., Allen, K. A., Yu, J., Koutavas, A., and Jaccard, S. L.: Deep-Sea Oxygen

494   Depletion and Ocean Carbon Sequestration During the Last Ice Age, Global Biogeochem Cycles, 33, 301–317,

495   https://doi.org/https://doi.org/10.1029/, 2019.

496   Babbin, A. R., Babbin, A. R., Keil, R. G., Devol, A. H., and Ward, B. B.: Oxygen Control Nitrogen Loss in the Ocean, 406,

497   https://doi.org/10.1126/science.1248364, 2014.

498   Bakun, A. and Nelson, C. S.: The seasonal cycle of wind-stress curl in subtropical eastern boundary current regions, J.

499   Physical Oceanography, 21, 1815–1834, https://doi.org/10.1175/1520-0485(1991)021<1815:TSCOWS>2.0.CO;2, 1991.

500   Bograd, S. J., Castro, C. G., di Lorenzo, E., Palacios, D. M., Bailey, H., Gilly, W., and Chavez, F. P.: Oxygen declines and

501   the shoaling of the hypoxic boundary in the California Current, Geophys Res Lett, 35, 1–6,

502   https://doi.org/10.1029/2008GL034185, 2008.

503   Bograd, S. J., Schroeder, I., Sarkar, N., Qiu, X., Sydeman, W. J., and Schwing, F. B.: Phenology of coastal upwelling in the

504   California Current, Geophys Res Lett, 36, 1–5, https://doi.org/10.1029/2008GL035933, 2009.

505   Brunner, B., Contreras, S., Lehmann, M. F., Matantseva, O., Rollog, M., and Kalvelage, T.: Nitrogen isotope effects induced

506   by anammox bacteria, 2–7, https://doi.org/10.1073/pnas.1310488110, 2013.

507   Canuel, E. A. and Martens, C. S.: Reactivity of recently deposited organic matter : near the sediment-water Degradation

508   interface of lipid compounds, 60, 1793–1806, 1996.

509   Cartapanis, O., Tachikawa, K., and Bard, E.: Northeastern Pacific oxygen minimum zone variability over the past 70 kyr :

510   Impact of biological production and oceanic ventilation, 26, 1–17, https://doi.org/10.1029/2011PA002126, 2011.

511   Castro, C. G., Chavez, F. P., and Collins, C. A.: Role of the California undercurrent in the export of denitrified waters from

512   the eastern tropical North Pacific, Global Biogeochem Cycles, 15, 819–830, https://doi.org/10.1029/2000GB001324, 2001.

513   Chavez, F. P. and Messié, M.: A comparison of Eastern Boundary Upwelling Ecosystems, Prog Oceanogr, 83, 80–96,

514   https://doi.org/10.1016/j.pocean.2009.07.032, 2009.

515 Checkley, D. M. and Barth, J. A.: Patterns and processes in the California Current System, Prog Oceanogr, 83, 49–64,

516 https://doi.org/10.1016/j.pocean.2009.07.028, 2009.

517 Choumiline, K., Pérez-Cruz, L., Gray, A. B., Bates, S. M., and Lyons, T. W.: Scenarios of Deoxygenation of the Eastern

518 Tropical North Pacific During the Past Millennium as a Window Into the Future of Oxygen Minimum Zones, Front Earth Sci

519 (Lausanne), 7, 1–23, https://doi.org/10.3389/feart.2019.00237, 2019.

520 Codispoti, L. A., Brandes, J. A., Christensen, J. P., Devol, A. H., Naqvi, S. W. A., Paerl, H. W., and Yoshinari, T.: The

521 oceanic fixed nitrogen and nitrous oxide budgets: Moving targets as we enter the anthropocene?, Sci Mar, 65, 85–105,

522 https://doi.org/10.3989/scimar.2001.65s285, 2001.

523 Dalsgaard, T., Thamdrup, B., Farías, L., and Revsbech, N. P.: Anammox and denitrification in the oxygen minimum zone of

524 the eastern South Pacific, Limnol Oceanogr, 57, 1331–1346, https://doi.org/10.4319/lo.2012.57.5.1331, 2012.

525 Dorman, C. E. and Winanat, C. D.: Buoy observations of the atmosphere along the west coast of the United States, 1981-

526 1990, J Geophys Res, 100, 1981–1990, https://doi.org/10.1029/95jc00964, 1995.

527 Fine, R. A., Maillet, K. A., Sullivan, K. F., and Willey, D.: Circulation and Ventilation flux of the Pacific Ocean, J Geophys

528 Res Oceans, 106, 22159–22178, https://doi.org/10.1029/1999jc000184, 2001.

529 Frigstad, H., Andersen, T., Hessen, D. O., Naustvoll, L. J., Johnsen, T. M., and Bellerby, R. G. J.: Seasonal variation in

530 marine C:N:P stoichiometry: Can the composition of seston explain stable Redfield ratios?, Biogeosciences, 8, 2917–2933,

531 https://doi.org/10.5194/bg-8-2917-2011, 2011.

532 Fu, W., Bardin, A., and Primeau, F.: Tracing ventilation source of tropical pacific oxygen minimum zones with an adjoint

533 global ocean transport model, Deep Sea Res 1 Oceanogr Res Pap, 139, 95–103, https://doi.org/10.1016/j.dsr.2018.07.017,

534 2018.

535 Galán, A., Molina, V., Thamdrup, B., Woebken, D., Lavik, G., Kuypers, M. M. M., and Ulloa, O.: Anammox bacteria and

536 the anaerobic oxidation of ammonium in the oxygen minimum zone off northern Chile, Deep Sea Res 2 Top Stud Oceanogr,

537 56, 1021–1031, https://doi.org/10.1016/j.dsr2.2008.09.016, 2009.

538 Ganeshram, R. S., Pedersen, T. F., Calvert, S. E., McNeill, G. W., and Fontugne, M. R.: Glacial-interglacial variability in

539 denitrification in the World's Oceans : Causes and consequences, Paleoceanography, 15, 361–367, 2000.

van de Graaf, A. A., Mulder, A., de Bruijn, P., Jetten, M. S. M., Robertson, L. A., and Kuenen, J. G.: Anaerobic oxidation of ammonium is a biologically mediated process, Appl Environ Microbiol, 61, 1246–1251, https://doi.org/10.1128/aem.61.4.1246-1251.1995, 1995.

van de Graaf, A. A., de Bruijn, P., Robertson, L. A., Jetten, M. S. M., and Kuenen, J. G.: Metabolic pathway of anaerobic ammonium oxidation on the basis of 15N studies in a fluidized bed reactor, Microbiology (N Y), 143, 2415–2421, https://doi.org/10.1099/00221287-143-7-2415, 1997.

Gruber, N.: The Ocean Carbon Cycle and Climate, in: The Ocean Carbon Cycle and Climate, edited by: Follows, M. and Oguz, T., Dordrecht, https://doi.org/10.1007/978-1-4020-2087-2, 2004.

Hamasaki, K., Shishikura, R., Suzuki, S., Shiozaki, T., Ogawa, H., Nakamura, T., and Suwa, Y.: Distribution and phylogeny of anaerobic ammonium-oxidizing (anammox) bacteria in the water column of the central Pacific Ocean, Deep Sea Res 2 Top Stud Oceanogr, 156, 60–67, https://doi.org/10.1016/j.dsr2.2017.11.013, 2018.

Hamersley, M. R., Lavik, G., Woebken, D., Rattray, J. E., Lam, P., Hopmans, E. C., Sinninghe Damsté, J. S., Krüger, S., Graco, M., Gutiérrez, D., and Kuypers, M. M. M.: Anaerobic ammonium oxidation in the Peruvian oxygen minimum zone, Limnol Oceanogr, 52, 923–933, https://doi.org/10.4319/lo.2007.52.3.0923, 2007.

Hendy, I. L. and Kennett, J. P.: Tropical forcing of North Pacific intermediate water distribution during Late Quaternary rapid climate change?, Quat Sci Rev, 22, 673–689, https://doi.org/10.1016/S0277-3791(02)00186-5, 2003.

Hendy, I. L. and Pedersen, T. F.: Oxygen minimum zone expansion in the Eastern Tropical North Pacific during deglaciation, Geophys Res Lett, 33, 1–5, https://doi.org/10.1029/2006GL025975, 2006.

Herbert, T. D., Schuffert, J. D., Andreasen, D., Heusser, L., Lyle, M., Mix, A., Ravelo, A. C., Stott, L. D., and Herguera, J. C.: Collapse of the California current during glacial maxima linked to climate change on land, Science (1979), 293, 71–76, https://doi.org/10.1126/science.1059209, 2001.

Herguera, J. C., Herbert, T., Kashgarian, M., and Charles, C.: Intermediate and deep water mass distribution in the Pacific during the Last Glacial Maximum inferred from oxygen and carbon stable isotopes, Quat Sci Rev, 29, 1228–1245, https://doi.org/10.1016/j.quascirev.2010.02.009, 2010.

Hopmans, E. C., Kienhuis, M. V. V., Rattray, J. E., Jaeschke, A., Schouten, S., and Sinninghe Damsté, J. S.: Improved analysis of ladderane lipids in biomass and sediments using high-performance liquid chromatography/atmospheric pressure

chemical ionization tandem mass spectrometry, Rapid Communications in Mass Spectrometry, 20, 2099–2103, https://doi.org/10.1002/rcm, 2006.

Huyer, A.: Coastal upwelling in the California current system, Prog Oceanogr, 12, 259–284, https://doi.org/10.1016/0079-6611(83)90010-1, 1983.

Jaeschke, A., Ziegler, M., Hopmans, E. C., Reichart, G. J., Lourens, L. J., and Schouten, S.: Molecular fossil evidence for anaerobic ammonium oxidation in the Arabian Sea over the last glacial cycle, Paleoceanography, 24, https://doi.org/10.1029/2008PA001712, 2009.

Kalvelage, T., Lavik, G., Lam, P., Contreras, S., Arteaga, L., Löscher, C. R., Oschlies, A., Paulmier, A., Stramma, L., and Kuypers, M. M. M.: Nitrogen cycling driven by organic matter export in the South Pacific oxygen minimum zone, Nat Geosci, 6, 228–234, https://doi.org/10.1038/ngeo1739, 2013.

Van Kemenade, Z. R., Villanueva, L., Hopmans, E. C., Kraal, P., Witte, H. J., Sinninghe Damsté, J. S., and Rush, D.: Bacteriohopanetetrol-x: Constraining its application as a lipid biomarker for marine anammox using the water column oxygen gradient of the Benguela upwelling system, Biogeosciences, 19, 201–221, https://doi.org/10.5194/bg-19-201-2022, 2022.

van Kemenade, Z. R., Cutmore, A., Hennekam, R., Hopmans, E. C., van der Meer, M. T. J., Mojtahid, M., Jorissen, F. J., Bale, N. J., Reichart, G. J., Sinninghe Damsté, J. S., and Rush, D.: Marine nitrogen cycling dynamics under altering redox conditions: Insights from deposition of sapropels S1 and the ambiguous S2 in the Eastern Mediterranean Sea, Geochim Cosmochim Acta, 354, 197–210, https://doi.org/10.1016/j.gca.2023.06.018, 2023.

Kemp, A. E. S., Langhorne, D. N., Fairchild, I. J., Schmitt, T. S., and Nisbet, E. G.: Evidence for abrupt climate changes in annually laminated marine sediments, Philosophical Transactions of the Royal Society A: Mathematical, Physical and Engineering Sciences, 361, 1851–1870, https://doi.org/10.1098/rsta.2003.1247, 2003.

Kienast, S. S., Calvert, S. E., and Pedersen, T. F.: Nitrogen isotope and productivity variations along the northeast Pacific margin over the last 120 kyr: Surface and subsurface paleoceanography, Paleoceanography, 17, 7-1-7–17, https://doi.org/10.1029/2001PA000650, 2002.

Kobayashi, K., Makabe, A., Yano, M., Oshiki, M., Kindaichi, T., Casciotti, K. L., and Okabe, S.: Dual nitrogen and oxygen isotope fractionation during anaerobic ammonium oxidation by anammox bacteria, ISME Journal, 13, 2426–2436, https://doi.org/10.1038/s41396-019-0440-x, 2019.

593   Koeve, W. and Kähler, P.: Heterotrophic denitrification vs. autotrophic anammox-quantifying collateral effects on the

594   oceanic carbon cycle, Biogeosciences, 7, 2327–2337, https://doi.org/10.5194/bg-7-2327-2010, 2010.

595   Kuenen, J. G. and Robertson, L. A.: Ecology of Nitrification and Denitrification-Book.Pdf, in: The Nitrogen and Sulphur

596   Cycles, edited by: Cole, J. A. and Ferguson, S., Cambridge University Press, 162–218, 1987.

597   Kuypers, M. M. M., Silekers, A. O., Lavik, G., Schmid, M., Jøorgensen, B. B., Kuenen, J. G., Sinninghe Damsté, J. S.,

598   Strous, M., and Jetten, M. S. M.: Anaerobic ammonium oxidation by anammox bacteria in the Black Sea, Nature, 422, 608–

599   611, https://doi.org/10.1038/nature01472, 2003.

600   Laffoley, D. and Baxter, J. M.: Ocean deoxygenation : everyone's problem. Summary for policy makers,

601   https://doi.org/10.2305/iucn.ch.2019.14.en, 2019.

602   Lamb, A. L., Wilson, G. P., and Leng, M. J.: A review of coastal palaeoclimate and relative sea-level reconstructions using

603   δ13C and C/N ratios in organic material, Earth Sci Rev, 75, 29–57, https://doi.org/10.1016/j.earscirev.2005.10.003, 2006.

604   Lembke-Jene, L., Tiedemann, R., Nürnberg, D., Gong, X., and Lohmann, G.: Rapid shift and millennial-scale variations in

605   Holocene North pacific intermediate water ventilation, Proc Natl Acad Sci U S A, 115, 5365–5370,

606   https://doi.org/10.1073/pnas.1714754115, 2018.

607   Liu, Z., Altabet, M. A., and Herbert, T. D.: Glacial-interglacial modulation of eastern tropical North Pacific denitrification

608   over the last 1.8-Myr, Geophys Res Lett, 32, 1–4, https://doi.org/10.1029/2005GL024439, 2005.

609   Lu, Z., Hoogakker, B. A. A., Hillenbrand, C. D., Zhou, X., Thomas, E., Gutchess, K. M., Lu, W., Jones, L., and Rickaby, R.

610   E. M.: Oxygen depletion recorded in upper waters of the glacial Southern Ocean, Nat Commun, 48,

611   https://doi.org/10.1038/ncomms11146, 2016.

612   Lyle, M., Koizumi, I., Richter, C., Fox, P. J., Baldau, J., and Francis, T. J. G.: Proceedings of the Ocean Drilling Program,

613   https://doi.org/10.1097/BLO.0b013e3181576080, 1997.

614   Matsumoto, K., Tanioka, T., and Rickaby, R.: Linkages between dynamic phytoplankton c:N:P and the ocean carbon cycle

615   under climate change, Oceanography, 33, 44–52, https://doi.org/10.5670/oceanog.2020.203, 2020.

616   Matul, A., Abelmann, A., Khusid, T., Chekhovskaya, M., Kaiser, A., Nürnberg, D., and Tiedemann, R.: Late Quaternary

617   changes of the oxygen conditions in the bottom and intermediate waters on the western Kamchatka continental slope, the Sea

618   of Okhotsk, Deep Sea Res 2 Top Stud Oceanogr, 125–126, 184–190, https://doi.org/10.1016/j.dsr2.2013.03.023, 2016.

619   Nicholson, S. E. and Flohn, H.: African climatic changes in late Pleistocene and Holocene and the general atmospheric

620   circulation., Sea level, ice and climatic change. Proc. Canberra symposium, December 1979, 2, 295–301, 1981.

621   Ortiz, J., Mix, A., Hostetler, S., and Kashgarian, M.: The California Current of the Last Glacial Maximum: Reconstruction at

622   42°N based on multiple proxies, Paleoceanography, 12, 191–205, https://doi.org/10.1029/96PA03165, 1997.

623   Paulmier, A. and Ruiz-Pino, D.: Oxygen minimum zones (OMZs) in the modern ocean, Prog Oceanogr, 80, 113–128,

624   https://doi.org/10.1016/j.pocean.2008.08.001, 2009.

625   Peng, X., Fuchsman, C. A., Jayakumar, A., Oleynik, S., Martens-Habbema, W., Devol, A. H., and Ward, B. B.: Ammonia

626   and nitrite oxidation in the Eastern tropical North Pacific, Global Biogeochem Cycles, 29, 2034–2049,

627   https://doi.org/10.1002/2015GB005278, 2015.

628   Peters, B., Horak, R., Devol, A., Fuchsman, C., Forbes, M., Mordy, C. W., and Casciotti, K. L.: Estimating fixed nitrogen

629   loss and associated isotope effects using concentration and isotope measurements of NO3–, NO2–, and N2 from the Eastern

630   Tropical South Pacific oxygen deficient zone, Deep Sea Res 2 Top Stud Oceanogr, 156, 121–136,

631   https://doi.org/10.1016/j.dsr2.2018.02.011, 2018.

632   Pierce, S. D., Barth, J. A., Kipp Shearman, R., and Erofeev, A. Y.: Declining oxygen in the northeast Pacific, J Phys

633   Oceanogr, 42, 495–501, https://doi.org/10.1175/JPO-D-11-0170.1, 2012.

634   Placencia, J. A., Garcés-Vargas, J., Lange, C. B., and Hebbeln, D.: Alkenone-based temperature patterns along the eastern

635   South Pacific Coastal Ocean: the effect of upwelling and advection on the sedimentary alkenone unsaturation-index

636   (U37K'), Biogeosciences Discussions, 7, 545–564, 2010.

637   Rattray, J. E., Van De Vossenberg, J., Hopmans, E. C., Kartal, B., Van Niftrik, L., Rijpstra, W. I. C., Strous, M., Jetten, M.

638   S. M., Schouten, S., and Damsté, J. S. S.: Ladderane lipid distribution in four genera of anammox bacteria, Arch Microbiol,

639   190, 51–66, https://doi.org/10.1007/s00203-008-0364-8, 2008.

640   Rattray, J. E., Van Vossenberg, J. De, Jaeschke, A., Hopmans, E. C., Wakeham, S. G., Lavik, G., Kuypers, M. M. M.,

641   Strous, M., Jetten, M. S. M., Schouten, S., and Sinninghe Damsté, J. S.: Impact of temperature on ladderane lipid distribution

642   in anammox bacteria, Appl Environ Microbiol, 76, 1596–1603, https://doi.org/10.1128/AEM.01796-09, 2010.

643   Reid, J. L.: On the total geostrophic circulation of the pacific ocean : flow patterns , tracers , and transports, 39, 263–352,

644   1997.

Reid, J. L. and Mantyla, A. W.: On the Mid-Depth Circulation of the North Pacific Ocean, J Phys Oceanogr, 8, 946–951, https://doi.org/10.1175/1520-0485(1978)008<0946:otmdco>2.0.co;2, 1978.

Robinson, R. S., Kienast, M., Albuquerque, A. L., Altabet, M., Contreras, S., Holz, R. D. P., Dubois, N., Francois, R., Galbraith, E., Hsu, T., Ivanochko, T., Jaccard, S., Kao, S., Kiefer, T., Kienast, S., Lehmann, M., Martinez, P., Mccarthy, M., Möbius, J., Pedersen, T., Quan, T. M., Ryabenko, E., Schmittner, A., Schneider, R., and Schneider-mor, A.: A review of nitrogen isotopic alteration in marine sediments, 27, https://doi.org/10.1029/2012PA002321, 2012.

Rush, D. and Sinninghe Damsté, J. S.: Lipids as paleomarkers to constrain the marine nitrogen cycle, Environ Microbiol, 19, 2119–2132, https://doi.org/10.1111/1462-2920.13682, 2017.

Rush, D., Jaeschke, A., Hopmans, E. C., Geenevasen, J. A. J., Schouten, S., and Damsté, J. S. S.: Short chain ladderanes: Oxic biodegradation products of anammox lipids, Geochim Cosmochim Acta, 75, 1662–1671, https://doi.org/10.1016/j.gca.2011.01.013, 2011.

Rush, D., Wakeham, S. G., Hopmans, E. C., Schouten, S., and Sinninghe Damsté, J. S.: Biomarker evidence for anammox in the oxygen minimum zone of the Eastern Tropical North Pacific, Org Geochem, 53, 80–87, https://doi.org/10.1016/j.orggeochem.2012.02.005, 2012a.

Rush, D., Hopmans, E. C., Wakeham, S. G., Schouten, S., and Damst, J. S. S.: Occurrence and distribution of ladderane oxidation products in different oceanic regimes, 2407–2418, https://doi.org/10.5194/bg-9-2407-2012, 2012b.

Rush, D., Hopmans, E. C., Wakeham, S. G., Schouten, S., and Sinninghe Damsté, J. S.: Occurrence and distribution of ladderane oxidation products in different oceanic regimes, Biogeosciences, 9, 2407–2418, https://doi.org/10.5194/bg-9-2407-2012, 2012c.

Rush, D., Talbot, H. M., Van Der Meer, M. T. J., Hopmans, E. C., Douglas, B., and Damsté, J. S. S.: Biomarker evidence for the occurrence of anaerobic ammonium oxidation in the eastern Mediterranean Sea during Quaternary and Pliocene sapropel formation, Biogeosciences, 16, 2467–2479, https://doi.org/10.5194/bg-16-2467-2019, 2019.

Ryabenko, E.: Stable Isotope Methods for the Study of the Nitrogen Cycle, in: Topics in Oceanography, edited by: Zambianchi, E., 49–88, https://doi.org/10.5772/56105, 2013.

Sahu, S., Allen, S. E., Saldías, G. S., Klymak, J. M., and Zhai, L.: Spatial and Temporal Origins of the La Perouse Low Oxygen Pool: A Combined Lagrangian Statistical Approach, J Geophys Res Oceans, 127, 1–20, https://doi.org/10.1029/2021JC018135, 2022.

Schneider, B., Schlitzer, R., Fischer, G., and Nöthig, E. M.: Depth-dependent elemental compositions of particulate organic matter (POM) in the ocean, Global Biogeochem Cycles, 17, https://doi.org/10.1029/2002gb001871, 2003.

Sigman, D. M. and Fripiat, F.: Nitrogen isotopes in the ocean, in: Encyclopedia of Ocean Sciences, edited by: Kirk Cochran, J., Bokuniewicz, H. J., and Yager, P. L., Elsevier Ltd, 263–278, https://doi.org/10.1016/B978-0-12-409548-9.11605-7, 2019.

Sinninghe Damsté, J. S., Strous, M., Rijpstra, W. I. C., Hopmans, E. C., Geenevasen, J. A. J., Van Duin, A. C. T., Van Niftrik, L. A., and Jetten, M. S. M.: Linearly concatenated cyclobutane lipids form a dense bacterial membrane, Nature, 419, 708–712, https://doi.org/10.1038/nature01067, 2002.

Smith, K. L., Messié, M., Connolly, T. P., and Huffard, C. L.: Decadal Time-Series Depletion of Dissolved Oxygen at Abyssal Depths in the Northeast Pacific, Geophys Res Lett, 49, https://doi.org/10.1029/2022GL101018, 2022.

Sollai, M., Hopmans, E. C., Schouten, S., Keil, R. G., and Sinninghe Damsté, J. S.: Intact polar lipids of Thaumarchaeota and anammox bacteria as indicators of N cycling in the eastern tropical North Pacific oxygen-deficient zone, Biogeosciences, 12, 4725–4737, https://doi.org/10.5194/bg-12-4725-2015, 2015.

Sonnerup, R. E., Quay, P. D., and Bullister, J. L.: Thermocline ventilation and oxygen utilization rates in the subtropical North Pacific based on CFC distributions during WOCE, Deep Sea Res 1 Oceanogr Res Pap, 46, 777–805, https://doi.org/10.1016/S0967-0637(98)00092-2, 1999.

Stramma, L., Johnson, G. C., Firing, E., and Schmidtko, S.: Eastern Pacific oxygen minimum zones: Supply paths and multidecadal changes, J Geophys Res Oceans, 115, 1–12, https://doi.org/10.1029/2009JC005976, 2010.

Tesdal, J. E., Galbraith, E. D., and Kienast, M.: Nitrogen isotopes in bulk marine sediment: Linking seafloor observations with subseafloor records, Biogeosciences, 10, 101–118, https://doi.org/10.5194/bg-10-101-2013, 2013.

Thamdrup, B., Dalsgaard, T., Jensen, M. M., Ulloa, O., Farías, L., and Escribano, R.: Anaerobic ammonium oxidation in the oxygen-deficient waters off northern Chile, Limnol Oceanogr, 51, 2145–2156, https://doi.org/10.4319/lo.2006.51.5.2145, 2006.

Thomson, R. E. and Krassovski, M. V.: Poleward reach of the California Undercurrent extension, J Geophys Res Oceans, 115, https://doi.org/10.1029/2010JC006280, 2010.

Thunell, R. C. and Kepple, A. B.: Glacial-Holocene D15N record from the Gulf of Tehuantepec, Mexico: Implications for denitrification in the eastern equatorial Pacific and changes in atmospheric N2O, Global Biogeochem Cycles, 18, https://doi.org/10.1029/2002GB002028, 2004.

Vallero, D. A.: Air pollution biogeochemistry, in: Air Pollution Calculations, edited by: Vallero, D. A., Elsevier, 175–206, https://doi.org/10.1016/b978-0-12-814934-8.00008-9, 2019.

Verardo, D. J. and Mcintyre, A.: AMERIiA) I, 9, 63–86, 1994.

Vossenberg, J. Van De, Rattray, J. E., Geerts, W., Kartal, B., Niftrik, L. Van, Donselaar, E. G. Van, Damsté, J. S. S., Strous, M., and Jetten, M. S. M.: Enrichment and characterization of marine anammox bacteria associated with global nitrogen gas production, 10, 3120–3129, https://doi.org/10.1111/j.1462-2920.2008.01643.x, 2008.

Wang, Y., Hendy, I. L., and Zhu, J.: Expansion of the Southern California oxygen minimum zone during the early-to mid-Holocene due to reduced ventilation of the Northeast Pacific, Quat Sci Rev, 238, 106326, https://doi.org/10.1016/j.quascirev.2020.106326, 2020.

Ward, B. B.: How nitrogen is lost, Science (1979), 341, 352–353, https://doi.org/10.1126/science.1240314, 2013.

White, M. E., Rafter, P. A., Stephens, B. M., Wankel, S. D., and Aluwihare, L. I.: Recent Increases in Water Column Denitrification in the Seasonally Suboxic Bottom Waters of the Santa Barbara Basin, Geophys Res Lett, 46, 6786–6795, https://doi.org/10.1029/2019GL082075, 2019.

Whitney, F. A., Freeland, H. J., and Robert, M.: Persistently declining oxygen levels in the interior waters of the eastern subarctic Pacific, Prog Oceanogr, 75, 179–199, https://doi.org/10.1016/j.pocean.2007.08.007, 2007.

Worne, S., Kender, S., Swann, G. E. A., Leng, M. J., and Ravelo, A. C.: Coupled climate and subarctic Pacific nutrient upwelling over the last 850,000 years, Earth Planet Sci Lett, 522, 87–97, https://doi.org/10.1016/j.epsl.2019.06.028, 2019.

Yamamoto, M., Yamamuro, M., and Tanaka, Y.: The California current system during the last 136,000 years: response of the North Pacific High to precessional forcing, Quat Sci Rev, 26, 405–414, https://doi.org/10.1016/j.quascirev.2006.07.014, 2007.

Zhou, Y., Gong, H., and Zhou, F.: Responses of Horizontally Expanding Oceanic Oxygen Minimum Zones to Climate Change Based on Observations, Geophys Res Lett, 49, 1–11, https://doi.org/10.1029/2022GL097724, 2022.

Zonneveld, K. A. F., Versteegh, G. J. M., Kasten, S., Eglinton, T. I., Emeis, K., Huguet, C., and Koch, B. P.: Selective preservation of organic matter in marine environments ; processes and impact on the sedimentary record, 483–511, 2010.